Available online at www.sciencedirect.com

SciVerse ScienceDirect

journal homepage: www.elsevier.com/locate/jmbbm

Research paper

Compressive behavior of a turtle's shell: Experiment, modeling, and simulation

R. Damiens[a], H. Rhee[a,b,*], Y. Hwang[c], S.J. Park[a], Y. Hammi[a,b], H. Lim[d], M.F. Horstemeyer[a,b]

[a] Center for Advanced Vehicular Systems, Mississippi State University, Mississippi State, MS 39762-5405, USA
[b] Department of Mechanical Engineering, Mississippi State University, Mississippi State, MS 39762-9552, USA
[c] Spirit AeroSystems, 3801 South Oliver Street, Wichita, KS 67210, USA
[d] Department of Mathematics and Statistics, Mississippi State University, Mississippi State, MS 39762-9715, USA

ARTICLE INFO

Article history:
Received 28 April 2011
Received in revised form
7 October 2011
Accepted 8 October 2011
Published online 18 November 2011

Keywords:
Turtle shell
Carapace
Compression test
Modeling
Simulation

ABSTRACT

The turtle's shell acts as a protective armor for the animal. By analyzing a turtle shell via finite element analysis, one can obtain the strength and stiffness attributes to help design man-made armor. As such, finite element analysis was performed on a *Terrapene carolina* box turtle shell. Experimental data from compression tests were generated to provide insight into the scute through-thickness behavior of the turtle shell. Three regimes can be classified in terms of constitutive modeling: linear elastic, perfectly inelastic, and densification regions, where hardening occurs. For each regime, we developed a model that comprises elasticity and densification theory for porous materials and obtained all the material parameters by correlating the model with experimental data. The different constitutive responses arise as the deformation proceeded through three distinctive layers of the turtle shell carapace. Overall, the phenomenological stress–strain behavior is similar to that of metallic foams.

1. Introduction

Biological structural materials have gained tremendous attention in recent years, because they exhibit mechanical properties that are far beyond those of their synthetic counterparts (Lin et al., 2006; Menig et al., 2000, 2001; Meyers et al., 2006). These exceptional mechanical properties are the result of their organization in terms of composition and structure. They contain both organic and inorganic components woven into complex structures that are hierarchically organized at the nanoscale, microscale, and mesoscale levels (Meyers et al., 2006). Studying biological materials and systems enables material scientists and engineers to develop biologically inspired designs. This field of study is also known as biomimetics, which is one of the new frontiers in materials science (Meyers et al., 2008). Many studies have been performed to discover the structure and mechanical properties of biological skeletons. For example, sea shells (Katti et al., 2001, 2004, 2005a,b, 2006; Katti and Katti, 2006; Lin et al., 2006; Menig et al., 2000, 2001; Meyers

* *Corresponding author at:* Center for Advanced Vehicular Systems, Mississippi State University, Mississippi State, MS 39762-5405, USA. Tel.: +1 662 3259221; fax: +1 662 3255433.
E-mail address: hrhee@cavs.msstate.edu (H. Rhee).

1751-6161/$ - see front matter © 2011 Elsevier Ltd. All rights reserved.
doi:10.1016/j.jmbbm.2011.10.011

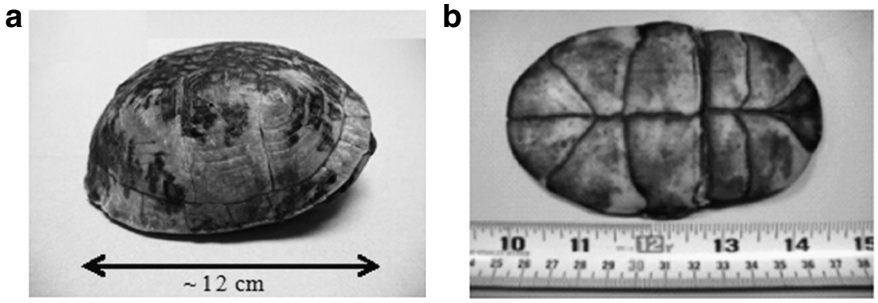

Fig. 1 – A macroscopic morphology of a turtle shell: (a) a dorsal view showing the upper shell (carapace), and (b) a ventral view showing the lower shell (plastron).

et al., 2006, 2008; Mohanty et al., 2006), bird beaks (Seki et al., 2006; Vecchio, 2005), crustacean exoskeletons (Raabe et al., 2005, 2006; Sachs et al., 2006), bones (Meyers et al., 2008), and teeth (Meyers et al., 2008) have been extensively studied. In addition, the structure of the soft suture between adjacent bone segments of the red-eared slider turtle shell and its supposed mechanical function have been discussed in a recent publication (Krauss et al., 2009). The authors concluded that the convoluted structure of the suture permits easy deformation at small loads while it provides stiffening upon larger deformations as a composite material with interlocking elements. However, studies on the turtle's armor system have not been undertaken to the best of our knowledge, particularly with respect to finite element analysis.

The primary function of the turtle shell is for armor defense against environmental penetration events. The shell has two sections: the upper or dorsal section is called the *carapace* and the lower or ventral section is called the *plastron* (Alderton, 1988), as shown in Fig. 1. The carapace and the plastron are connected by bridges that are located between the front and hind limbs on either side of the body. The carapace and the plastron comprise individual horny shields called *scutes*. The pattern in which they are assembled on the shell enhances the overall strength of the shell. The details of the structure of the turtle shell in different length scales will be discussed in Section 3.

The aim of this study is to understand the constitutive behavior of the turtle shell, develop a material model, and run finite element simulations of the through-thickness behavior. By studying the relationship between the microstructure of the turtle shell and its mechanical properties, one can hopefully understand new venues for designing man-made armor. In order to accomplish this task, experiments and modeling were performed that were focused on the upper shell (carapace) of a box turtle (*Terrapene carolina*). Rhee et al. (2009) reported the hierarchical structure and mechanical behavior of the turtle shell carapace. Based on previously reported experimental results, computational modeling and simulation on the mechanical behavior of the turtle shell carapace were carried out. The findings from the present study could aid in identifying the pathway to design bio-inspired synthetic composite materials.

2. Material and methods

In order to model and simulate the mechanical behavior of the turtle shell, multiscale structure and mechanical properties were quantified under different length scales by using such biological structural material obtained after the natural death of a box turtle. The structure of the turtle shell carapace was investigated by using an optical microscope. Also included for modeling and simulation efforts, but not presented here, was the structure obtained from a scanning electron microscope (SEM). The turtle shell carapace was sectioned by using a diamond saw and prepared for microstructure observations. Sectioned specimens were cleaned by an ultrasonic cleaner and then mounted in epoxy by using a cold mount technique to minimize the detrimental effects during preparation of these biological samples. After characterizing the microstructure under the optical microscope, mounted samples were then sputter-coated with gold and examined under the SEM.

Quasi-static compression tests were carried out to provide a fundamental database for the computational modeling and simulation. Such tests were conducted by using an Instron 5882 electromechanical test machine; the maximum load capacity of the load cell was 100 kN. All tests were carried out at room temperature with various strain rates ranging from 10^{-4} to 10^{0} s^{-1} by using coupon specimens detached from the turtle shell carapace. The details of the specimen preparation and experimental procedures used can be found elsewhere (Rhee et al., 2009).

3. Results and discussion

3.1. *Structure and micromechanical properties of turtle shell*

Microstructural observations revealed that the turtle shell is a multiphase composite material that is arranged in a multiscale hierarchy (Rhee et al., 2009). The turtle shell carapace is made of a sandwich composite structure, and such functionally graded material (FGM) is comprised of a relatively denser exterior that covers a network of fibrous foam interior, as shown in Fig. 2(a). These fibrous structures can be seen inside the cell upon closer observation.

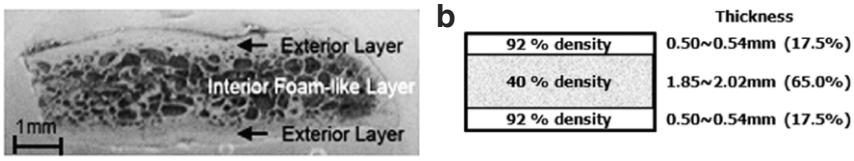

Fig. 2 – (a) A cross-sectional view of the turtle shell carapace showing composite layers, and (b) a schematic illustration of three distinctive layers' dimension and porosity level (converse of density) analysis.

The dimensions and porosities of three distinctive layers through the thickness were determined by utilizing in-house image analyzer software, and the results are shown in Fig. 2(b). Such information was used to construct material modeling and simulation efforts. The symmetric sandwich structure of the turtle shell carapace has 2.85–3.10 mm thickness. Each exterior layer has 17.5% (0.50–0.54 mm) of total thickness with 92% density (8% porosity) while the interior layer has 65.0% (1.85–2.02 mm) of total thickness with 40% (60% porosity) density.

The chemical analysis was performed by using an energy-dispersive X-ray (EDX) spectroscopy technique, and the results obtained from various surfaces of the turtle shell revealed that the outermost skin layer mainly consisted of fibrous protein called keratin. Unlike the outermost keratin layer, the material right underneath the keratin layer and the inside surface of the turtle shell carapace contained abundant additional minerals such as calcium, phosphorous, sodium, chlorine, and magnesium that are main components of the bone (Rhee et al., 2009).

Experimental results obtained from nano-indentation and micro-indentation tests on the side surfaces of the turtle shell carapace showed that the exterior layers and interior cell walls possess comparable hardness and modulus values (Rhee et al., 2009). The microstructure observation, chemical analysis, and indentation test results obtained from various locations of the turtle shell clearly revealed that the turtle shell carapace is made of a sandwich composite structure having exterior bone layers that cover an interior bony network of fibrous foam layer.

3.2. *Compression test*

For quasi-static compression tests, two different types of coupon specimen were prepared. One type included all three layers while the other type contained only a bony exterior layer. The average size of the coupon specimens for compression tests was about 1 cm × 1 cm, and the samples were reasonably flat under such dimensions. Each compression test was repeated at least three times and the results were averaged together to minimize the experimental variation. Distinctive mechanical behaviors with respect to different types of specimen were compared, and the data obtained from the tests is illustrated in Fig. 3. The five curves in Fig. 3(a) were obtained from the test specimens including all three layers (two exterior and an interior layers); whereas the six curves in Fig. 3(b) were obtained from the specimens only containing a relatively denser exterior layer. The top three curves (in symbols) of those six curves in Fig. 3(b) were obtained from thinner specimens and the bottom three curves (in lines) represent thicker specimens. The thickness difference between those two regimes was about 15%. The deformation mechanism of the turtle shell carapace under quasi-static compression tests can be explained by importing that of synthetic foams or honeycombs, since the fundamental structures of the test specimens are similar to those of such cellular solids. The turtle shell coupon specimens containing all three layers initially deformed in a linear elastic manner due to the cell wall bending at small strains (Gibson and Ashby, 1997). After the initial linear elastic deformation, a plateau of deformation was reached because of the buckling of the cell walls. Another period of linear deformation took place after such a plateau of deformation since a densification occurred, resulting in a rapid increase of compressive stress, as shown in Fig. 3(a). When comparing the specimens containing the exterior region only, the thicker specimens showed a similar deformation yet much weaker behavior than that which can be observed in the specimens including all three layers, whereas the thinner specimens showed almost a linear compressive deformation behavior simply because of the density and structure differences (Fig. 3(b)). This implies that most of discernible pores within the exterior layer are distributed near the region between the exterior layer and the interior foam layer.

The comparison of specific energy absorption obtained from the quasi-static compression test results was also reported by Rhee et al. (2009). The energy absorption ability of the turtle shell carapace increased with increasing strain rate for a given density level. The composite layers including all three layers showed better energy absorption ability compared to the exterior layer for any given strain rate. In addition, such composite layers exhibited a considerable deformation plateau, which is a model index of good energy absorbing materials. The combined information of stress–strain relations and energy absorption ability is very important for designing an optimum energy absorbing composite material.

3.3. *Modeling of compression tests*

We developed a phenomenological constitutive model for the compressive behavior of the turtle shell based on the three regions classified in Fig. 3(a).

- Region I: linear elastic behavior.
- Region II: perfectly inelastic behavior as a plateau.
- Region III: densification behavior.

Each region was modeled separately, as the following description elucidates.

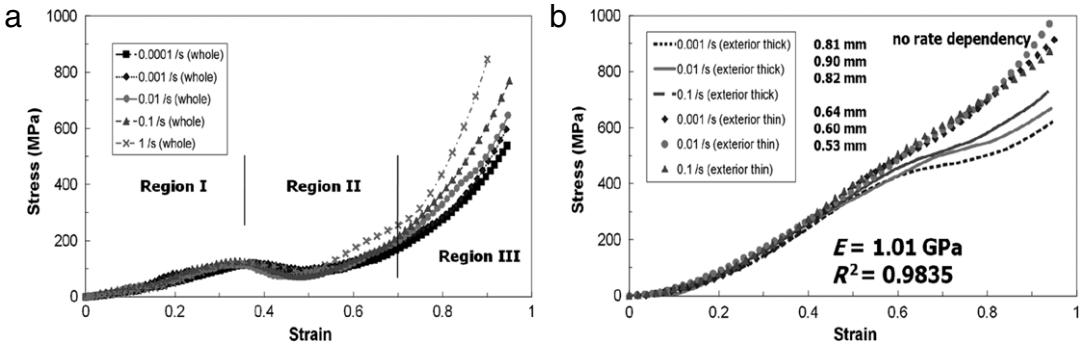

Fig. 3 – Compression test results on the coupon specimens: (a) including all three layers of the turtle shell carapace, and (b) only containing an exterior layer.

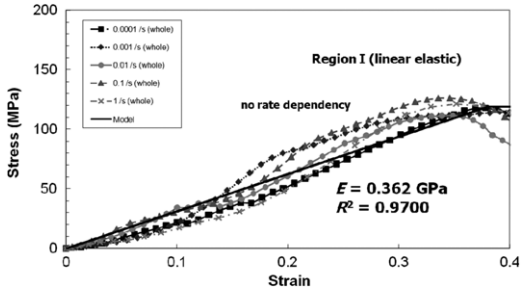

Fig. 4 – Stress–strain behavior of Region I in compression obtained from through-thickness turtle shell carapace showing a linear elastic deformation.

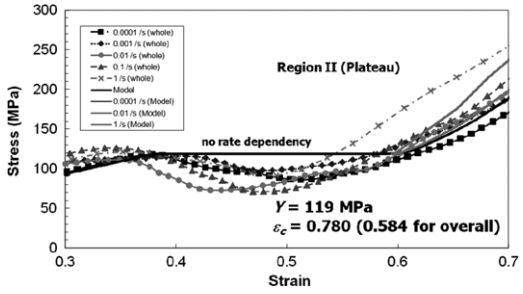

Fig. 5 – Stress–strain behavior of Region II in compression obtained from through-thickness turtle shell carapace showing stress drop-off.

Region I: This region is linear elastic for both skin and core layers, as shown in Figs. 3(a) and 4. There is essentially no strain rate dependence on compressive behavior in this region as five orders of magnitude of applied strain rates were imposed.

We adopted the model proposed by Panakkal et al. (1990) for elastic properties for porous materials. The model for the porous elastic modulus E based on the dense parent material elastic modulus E_0 used in this study is as follows:

$$E = E_0 \exp\left(-b\theta - c\theta^2\right), \tag{1}$$

where θ is the fractional porosity, that is, the fractional density $f = 1-\theta$, and b and c are constants that are determined via experiments.

We obtained $E_0 = 1.07$ GPa, $b = 0.95$, and $c = 1.00$ by correlating the results from two experiments: one was a compressive test for the skin layer as shown in Fig. 3(b), and the other one was a compressive test using the whole turtle shell thickness, as shown in Fig. 4. The elastic modulus obtained from the skin layer had much smaller values than those of various animal bones, probably due to the fact that the elastic modulus measurements strongly depend on the testing method, stress state, specimen orientation, etc. (Cowin, 1989; Hall, 1991, 1993; Hoffmeister et al., 2000; Tai et al., 2005; Goulet et al., 1994; Rhee et al., 2009). The Young's modulus obtained from the whole turtle shell thickness was also much smaller than that of human bone (Cowin, 1989; Panakkal et al., 1990) since the compression tests were carried out on the specimens containing all three sandwich composite layers including the porous core layer. Note that the exterior layer is linear elastic in all three regions. In Region I, we can model this region with three material parameters: E_0, b, and c.

Region II: This region is perfectly inelastic as a plateau as shown in Figs. 3(a) and 5. Similar to Region I, there is no rate dependence on the compressive behavior. We obtained a yield stress $Y = 119$ MPa by averaging all of the data at all of the strain rate levels. This yield phenomenon was only applied for the core layer while the skin layer was still linear elastic. The stress increased again after a certain amount of strain, which resulted in the onset of Region III. We call this the critical strain in which the main deformation occurred only in the core layer. We obtained the critical strain $\varepsilon_c = 0.780$ for the interior layer, that is 0.584 for the whole thickness, by using an averaging concept for data with all of the strain rates. In Region II, we can model this region with two material parameters Y and ε_c for the core layer. These parameters depend on the porosity of the core layer.

Region III: This region is a densification region after the plateau, as shown in Figs. 3(a) and 6. Unlike Regions I and II, there is a substantial strain rate dependence on the compressive behavior of the turtle shell. We used a quadratic function for the stress–strain relation in this region only for the interior region as follows:

$$\sigma = A(\varepsilon - \varepsilon_c)^2 + Y, \tag{2}$$

where σ is the engineering stress, ε is the engineering strain, and A is the material parameter. This parabolic function has

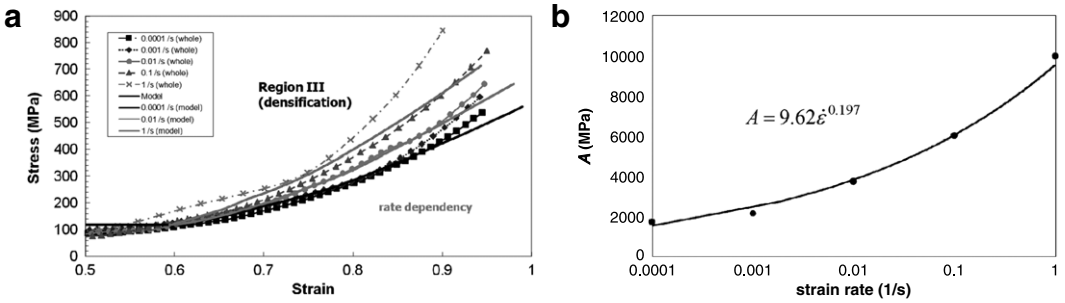

Fig. 6 – Stress–strain behavior of Region III in compression obtained from through-thickness turtle shell carapace showing the highly nonlinear work hardening: (a) compression response, and (b) rate dependence of A.

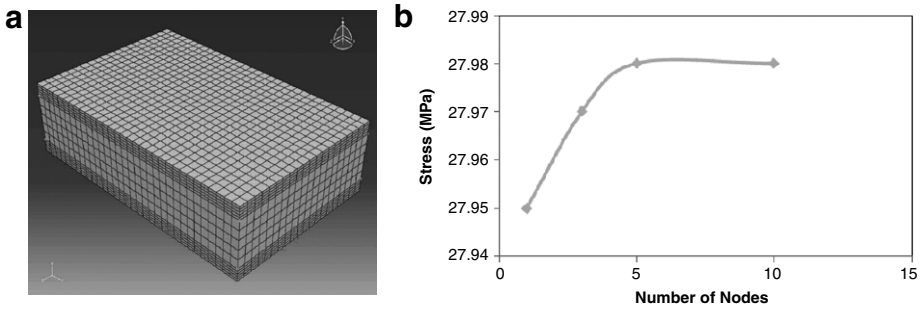

Fig. 7 – Simulation of compression test using ABAQUS: (a) mesh, and (b) mesh refinement simulations. Here, the number of nodes is increased for each of the three layers, so the number of nodes equaling 5 represents 15 nodes through the total thickness.

its vertex at the critical strain and the yield stress, (ε_c, Y). Material parameter A includes a rate dependence. We used the simple power law model, as follows:

$$A = A_0\dot{\varepsilon}^n, \tag{3}$$

where A_0 is the pre-exponent factor, and n is the exponent for the power law model. We obtained $A_0 = 9.52$ GPa and $n = 0.197$ with $R^2 = 0.996$ by correlating with the compressive

$$E = E_0 \exp(-b\theta - c\theta^2)$$

experimental data, as shown in Fig. 6(b). The R^2 value shows a good accuracy of the model with correlated parameters. In Region III, we can model this region with two material parameters A_0 and n for the core layer. These parameters depend on the porosity of the core layer.

3.4. *Simulation of compression tests*

Based on the developed model with seven parameters (E_0, b, and c for Region I, Y and ε_c for Region II, and A_0 and n for Region III) obtained from the previous section, we performed finite element analysis for the compressive tests using a commercial code, ABAQUS. We developed our own user subroutine of UMAT in ABAQUS with linear elements under small deformation and Cauchy stress tensor. In this subroutine UMAT, we used the yield stress Y for criteria between Regions I and II and the critical strain ε_c for criteria between Regions II and III in the interior layer. The model for the Poisson's ratio of porous material (υ) based on the Poisson's ratio of dense parent material (υ_0) used in this study is as follows (Gibson and Ashby, 1997):

$$\nu = \nu_0 (1 - \omega\theta), \tag{4}$$

where ω is a constant that is determined via experiments. In this study, we used literature values $\nu_0 = 0.31$ (Panakkal et al., 1990) and $\omega = 0.8$ (Gibson and Ashby, 1997).

Fig. 7(a) shows the typical mesh geometry used in this simulation. The number of nodal points in the thickness was determined by employing a mesh refinement study. Fig. 7(b) illustrates that the convergence of the solution was realized after about five nodal points for each of the three layers was employed. As such, the results are given from this level because the cost of more nodal points was much greater in terms of CPU time.

Fig. 8 provides the simulation results compared with the experimental results for three different strain rates. The results show good agreement between experiment data and simulation results. In the future, the tensile material properties will be obtained from three-point bending tests based on the model developed in this study for the compression test. In time, we will be able to simulate the compression test of the whole turtle shell.

4. Conclusions

For the first time, finite element analyses have been performed on a *Terrapene carolina* box turtle shell in order to understand the strength, stress–strain behavior, and

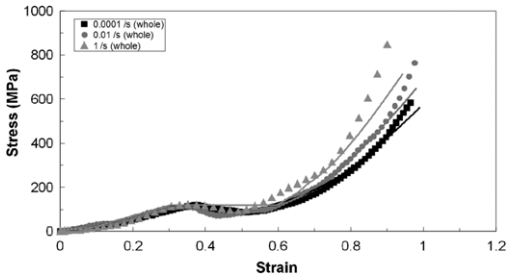

Fig. 8 – Comparison of finite element simulation results versus experimental data under compression at various strain rates for the through-thickness turtle shell.

overall stiffness. Finite element simulations were combined with compression experimental results to illustrate the gradients of porosity in the microstructure of the three-layered shell system. Compression test results showed a typical nonlinear deformation behavior similar to that of man-made foams. A three-phase constitutive model was developed and implemented in the finite element code ABAQUS, and it was used to capture the three regions of the stress–strain behavior. The three regions arose because of the three distinct layers through the thickness of the turtle shell. Experimental observations showed that the inner cell and outer layers of the shell were denser than the whole middle layer. This structure admits microbuckling of the middle layer first as the deformation proceeds. Now that this stage of the modeling has been performed, an overall shell analysis can be performed to study the geometric effects versus the material aspects of the turtle shell.

Acknowledgments

The authors would like to acknowledge the financial support for this work from the US Department of Energy (DOE) through the Southern Regional Center for Lightweight Innovative Design (SRCLID) program at Mississippi State University (Grant No. DE-FC26-06NT42755). This report was prepared as an account of work sponsored by an agency of the United States Government. Neither the United States Government nor any agency thereof, nor any of their employees, makes any warranty, express or implied, or assumes any legal liability or responsibility for the accuracy, completeness, or usefulness of any information, apparatus, product, or process disclosed, or represents that its use would not infringe privately owned rights. Reference herein to any specific commercial product, process, or service by trade name, trademark, manufacturer, or otherwise does not necessarily constitute or imply its endorsement, recommendation, or favoring by the United States Government or any agency thereof. The views and opinions of authors expressed herein do not necessarily state or reflect those of the United States Government or any agency thereof. The authors would also like to thank the DoD TARDEC SimBRS program for supporting this work.

REFERENCES

Alderton, D., 1988. Turtles & Tortoises of the World. Facts on File, New York, New York.

Cowin, S.C., 1989. Bone Mechanics. CRC Press, Inc., Boca Raton, Florida.

Gibson, L.J., Ashby, M.F., 1997. Cellular Solids: Structure and Properties, second ed. Cambridge University Press, Cambridge, U.K.

Goulet, R.W., Goldstein, S.A., Ciarelli, M.J., Kuhn, J.L., Brown, M.B., Feldkamp, L.A., 1994. The relationship between the structural and orthogonal compressive properties of trabecular bone. J. Biomech. 27, 375–389.

Hall, B.K., 1991. Bone: Bone Growth—A. CRC Press, Inc., Boca Raton, Florida.

Hall, B.K., 1993. Bone: Bone Growth—B. CRC Press, Inc., Boca Raton, Florida.

Hoffmeister, B.K., Smith, S.R., Handley, S.M., Rho, J.Y., 2000. Anisotropy of Young's modulus of human tibial cortical bone. Med. Biol. Eng. Comput. 38, 333–338.

Katti, K.S., Katti, D.R., 2006. Why is nacre so tough and strong? Mater. Sci. Eng. C 26, 1317–1324.

Katti, K.S., Katti, D.R., Pradhan, S.M., Bhosle, A., 2005b. Platelet interlocks are the key to toughness and strength in nacre. J. Mater. Res. 20, 1097–1100.

Katti, D.R., Katti, K.S., Sopp, J.M., Sarikaya, M., 2001. 3D finite element modeling of mechanical response in nacre-based hybrid nanocomposites. Comput. Theor. Polym. Sci. 11, 397–404.

Katti, K., Katti, D.R., Tang, J., Pradhan, S., Sarikaya, M., 2005a. Modeling mechanical responses in a laminated biocomposite—part II—nonlinear responses and nuances of nanostructure. J. Mater. Sci. 40, 1749–1755.

Katti, K.S., Mohanty, B., Katti, D.R., 2006. Nanomechanical properties of nacre. J. Mater. Res. 21, 1237–1242.

Katti, D.R., Pradhan, S.M., Katti, K.S., 2004. Modeling the organic–inorganic interfacial nanoasperities in a model bio-nanocomposite, nacre. Rev. Adv. Mater. Sci. 6, 162–168.

Krauss, S., Monsonego-Ornan, E., Zelzer, E., Fratzl, P., Shahar, R., 2009. Mechanical function of a complex three-dimensional suture joining the bony elements in the shell of the red-eared slider turtle. Adv. Mater. 21, 407–412.

Lin, A.Y.M., Meyers, M.A., Vecchio, K.S., 2006. Mechanical properties and structure of Strombus gigas, Tridacna gigas, and Haliotis rufescens sea shells: a comparative study. Mater. Sci. Eng. C 26, 1380–1389.

Menig, R., Meyers, M.H., Meyers, M.A., Vecchio, K.S., 2000. Quasi-static and dynamic mechanical response of Haliotis rufescens (abalone) shells. Acta Mater. 48, 2383–2398.

Menig, R., Meyers, M.H., Meyers, M.A., Vecchio, K.S., 2001. Quasi-static and dynamic mechanical response of Strombus gigis (conch) shells. Mater. Sci. Eng. A 297, 203–211.

Meyers, M.A., Chen, P.-Y., Lin, A.Y.-M., Seki, Y., 2008. Biological materials: structure and mechanical properties. Prog. Mater. Sci. 53, 1–206.

Meyers, M.A., Lin, A.Y.M., Seki, Y., Chen, P.-Y., Kad, B.K., Bodde, S., 2006. Structural biological composites: an overview. JOM 58, 35–41.

Mohanty, B., Katti, K.S., Katti, D.R., Verma, D., 2006. Dynamic nanomechanical response of nacre. J. Mater. Res. 21, 2045–2051.

Panakkal, J.P., Willems, H., Arnold, W., 1990. Nondestructive evaluation of elastic parameters of sintered iron powder compacts. J. Mater. Sci. 25, 1397–1402.

Raabe, D., Romano, P., Sachs, C., Fabritius, H., Al-Sawalmih, A., Yi, S.-B., Servos, G., Hartwig, H.G., 2006. Microstructure and crystallographic texture of the chitin–protein network in the biological composite material of the exoskeleton of the lobster Homarus Americanus. Mater. Sci. Eng. A 421, 143–153.

Raabe, D., Sachs, C., Romano, P., 2005. The crustacean exoskeleton as an example of a structurally and mechanically graded biological nanocomposite material. Acta Mater. 53, 4281–4292.

Rhee, H., Horstemeyer, M.F., Hwang, Y., Lim, H., El Kadiri, H., Trim, W., 2009. A study on the structure and mechanical behavior of the Terrapene carolina carapace: a pathway to design bio-inspired synthetic composites. Mater. Sci. Eng. C 29, 2333–2339.

Sachs, C., Fabritius, H., Raabe, D., 2006. Experimental investigation of the elastic–plastic deformation of mineralized lobster cuticle by digital image correlation. J. Struct. Biol. 155, 409–425.

Seki, Y., Kad, B., Benson, D., Meyers, M.A., 2006. The toucan beak: structure and mechanical response. Mater. Sci. Eng. C 26, 1412–1420.

Tai, K., Qi, H.J., Ortiz, C., 2005. Effect of mineral content on the nanoindentation properties and nanoscale deformation mechanisms of bovine tibial cortical bone. J. Mater. Sci., Mater. Med. 16, 947–959.

Vecchio, K.S., 2005. Synthetic multifunctional metallic–intermetallic laminate composites. JOM 57, 25–31.